J Mater Sci (2007) 42:779–783
DOI 10.1007/s10853-006-1440-6

Microstructure and magnetic properties of $Ni_{1-x}Zn_xFe_2O_4$ synthesized by combustion reaction

Ana Cristina F. M. Costa · Márcio R. Morelli · Ruth H. G. A. Kiminami

Received: 29 May 2003 / Accepted: 11 April 2006 / Published online: 13 January 2007

Abstract An investigation was made of samples having a chemical formula of $Ni_{1-x}Zn_xFe_2O_4$, where $x = 0.3$, 0.5 and 0.7. The samples were prepared by the reaction combustion synthesis method and sintered at 1,200 °C/2 h in a static air atmosphere. The influence of the Zn concentration on the relative density, microstructure and magnetic properties of the samples was studied. X-ray diffraction, scanning electron microscopy and magnetic hysteresis loop tracer were used to analyze the compositions. The samples were found to have a spinel cubic structure, sintered density of 92.9%–98.8% of the corresponding X-ray density, homogeneous microstructure with grain size ranging from 1.37 to 3.36 μm, maximum flux density of 0.16–0.35 T, field coercivity ranging from 17 to 168 A/m, and loss hysteresis of 1.5–105 W/kg. Increased grain growth, with fine pores inside the grains, was found to occur as the Zn concentration increased. The overall findings are discussed here in light of the existing understanding of these systems.

A. C. F. M. Costa
Department of Materials Engineering, Federal University of Paraíba, 58970-000 Campina Grande, PB, Brazil

M. R. Morelli · R. H. G. A. Kiminami (✉)
Department of Materials Engineering, Federal University of São Carlos, 13565-905 São Carlos, SP, Brazil
e-mail: ruth@power.ufscar.br

Introduction

A considerable amount of research in recent years has focused on zinc-substituted nickel ferrites because of their innumerable applications as non-resonant devices, radio frequency circuits, high-quality filters, rod antennas, transformer cores, read/write heads for high speed digital tape, and operating devices [1–4]. Polycrystalline ferrites are complex systems composed of crystallites, grain boundaries, and pores [5]. These ferrites' magnetic properties are determined by their chemical composition, porosity, grain size, etc. [2].

Depending on their applications, ferrites should have specific levels of magnetic parameters, most of which, such as the coercive field, initial magnetic permeability, threshold field, ferromagnetic resonance band, etc., do not depend solely on crystallochemical factors. These properties are very sensitive to the ferrite grains' microstructure, i.e., grain size and homogeneity, grain and boundary shapes, porosity and pore distribution, crystallographic texture, etc. [6].

Ni–Zn ferrites may be obtained by solid-state reaction of Fe_2O_3 and MO_x (M = Ni, Zn, Mg, Li, Cu, etc.). Therefore, because high temperature is required (>1,250 °C), the crystallite size, morphology and microscopic homogeneity of the final material are poorly controlled [7]. Hence, several synthesis procedures have been proposed, particularly for the control of particle size and morphology. Powders obtained by the combustion reaction method, in particular, display characteristics such as fine particle size, narrow particle size distribution, soft agglomerates, chemical purity and homogeneity, good crystallization, and low temperature products [8–10]. Unlike the solid-state reaction method, combustion reaction synthesis offers

additional advantages such as simple experimental setups, very short times from the reactants' preparation to the completion of the final product, savings in external energy consumption and the equally important potential of simplifying the processing prior to forming, offering a simple alternative to other elaborate techniques [11–17]. This study, therefore, investigated the influence of zinc concentrations on the microstructure and magnetic properties of Ni–Zn ferrites prepared by combustion reaction.

Experimental

Nanosize particle oxides of Ni–Zn ferrite with a nominal composition of $Ni_{1-x}Zn_xFe_2O_4$ ($x = 0.3$, 0.5 and 0.7% of the Zn) were prepared for combustion reaction using urea as fuel. The materials used were iron nitrate $-Fe(NO_3)_3{\cdot}9H_2O$ (Merck), zinc nitrate $-Zn(NO_3)_2{\cdot}6H_2O$ (Merck), nickel nitrate $-Ni(NO_3)_2{\cdot}6H_2O$ (Merck) and urea $-CO(NH_2)_2$ (Synth). Stoichiometric compositions of metal nitrate and urea were calculated using the total components' oxidizing and reducing valencies, which serve as the numerical coefficients for the stoichiometric balance, so that the equivalence ratio Φ_c is unity and the energy released is maximum [18].

The Ni–Zn ferrite powders obtained from the combustion reaction, with particle sizes of 18–26 nm [8–10], were uniaxially compacted by dry pressing under 392 MPa pressure into pellets (9.86 mm diameter) and toroids (17.0 mm outer diameter, 14.0 mm inner diameter and 4.0 mm thickness). The samples were sintered in air at 1,200 °C for 2 h. The powder and Ni–Zn ferrite samples sintered at 1,200 °C/2 h were characterized by X-ray diffraction (Kristaloflex D5000, CuK_α with a Ni filter, and scanning speed of 2° 2θ/min, in a 2θ range of 20–60°). The apparent density was calculated using the Archimedean principle. *B–H* loop measurements were taken of toroids with primary and secondary windings of 26 SWG enameled copper wire, using a hysteresis loop tracer (TCH 8600-B). This hysteresis loop allows one to determine the values of coercive force, H_c, maximum flux density, B_{max}, remanent flux density, B_r, and loss hysteresis, P_H. The following conditions were adopted to develop this work: a frequency of 1 kHz, applied magnetic field of 2,000 A/m, average toroid height of 4.0 mm and trapezoidal wave-shape induction. The frequency and the applied magnetic field values used here were chosen because of the limitations of the magnetic hysteresis loop tracer (TCH860034). All the measurements were taken at room temperature. The as-prepared combustion reaction powders and the microstructures of the sintered samples' polished surfaces were analyzed by scanning electron microscopy (Philips XL30 FEG)—SEM and the average grain size was calculated from the image analyzing software MOCHA of Jandell.

Results

Figure 1 shows diffractograms of the $Ni_{0.7}Zn_{0.3}Fe_2O_4$ (S3), $Ni_{0.5}Zn_{0.5}Fe_2O_4$ (S5) and $Ni_{0.3}Zn_{0.7}Fe_2O_4$ (S7) systems after synthesis and sintering at 1,200 °C/2 h. The X-ray diffraction of the S5 and S7 powders revealed cubic spinel Ni–Zn ferrite as the major phase and a small amount of hematite (α-Fe_2O_3) as the secondary phase. However, the S3 powder system showed single-phase cubic spinel Ni–Zn ferrite. The

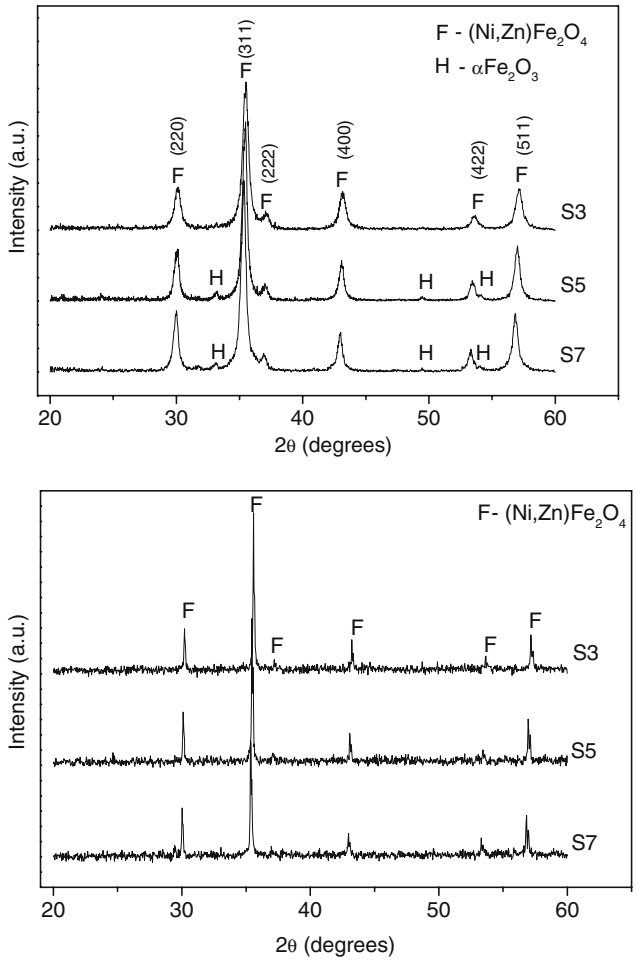

Fig. 1 X-ray diffractogram of the samples for the systems-$Ni_{0.7}Zn_{0.3}Fe_2O_4$ (S3), $Ni_{0.5}Zn_{0.5}Fe_2O_4$ (S5) and $Ni_{0.3}Zn_{0.7}Fe_2O_4$ (S7); (**a**) after combustion reaction and (**b**) sinterized at 1,200 °C/2 h

constant values of the lattice calculated for different Zn concentrations are given Table 1. The constant lattice apparently increased linearly with the Zn concentration in the $Ni_{1-x}Zn_xFe_2O_4$ system. In all the systems, the diffractograms of the samples after sintering at 1,200 °C/2 h confirmed the presence of the single-phase cubic spinel Ni–Zn ferrite, without the presence of the hematite phase. During sintering, the small amount of free hematite visible in the diffractograms of the S5 and S7 powders' systems reacted, by reactive sintering, into crystalline single-phase cubic spinel Ni–Zn ferrite. The Ni–Zn ferrite system showed a cubic spinel configuration with unit cells consisting of eight formula units of the form $(Zn_x^{2+} + Fe_{1-x}^{3+})[Ni_{1-x}^{2+} + Fe_{1+x}^{3+}]O_4^{2-}$.

Ni^{2+} ions show a marked preference for octahedral sites because of the favorable fit of these ions to charge distribution in the octahedral site crystal field. On the other hand, Zn^{2+} ions prefer tetrahedral sites due to their readiness to form covalent bonds involving sp^3 hybrid orbitals [19]. The linear increase of constant lattice found to occur with the Zn concentration may be attributed to the larger ionic radius of Zn^{2+} (0.84 Å) compared with the ionic radius of Ni^{2+} (0.74 Å). A similar linear variation of constant lattice with Zn concentrations has been observed by El-Sayed [5] for Ni–Zn ferrites prepared by the conventional oxide mixture method.

Figure 2 shows the micrographs obtained by scanning electron microscopy (SEM) for the samples of the S3, S5 and S7 systems sintered at 1,200 °C/2 h. The $Ni_{1-x}Zn_xFe_2O_4$ system's porosity was generally found to increase, accompanied by a decrease in grain size and a consequent reduction in the samples' density with increasing concentrations of Zn^{2+}.

The S3 system, Fig. 2a, displayed a homogeneous microstructure with a narrow grain size distribution, approximately hexagonal grains, average grain size of 3.36 μm and intergranular porosity (≈0.29 μm). The pellets' apparent density and apparent porosity were, respectively, 5.17 g/cm^3 (98.8% of the theoretical density) and 1.00 (Table 1). Figure 2b illustrates the microstructure of the S5 system's samples, revealing a homogeneous microstructure with narrow grain size distribution. The grains possess a hexagonal shape and an average grain size of 2.9 μm. Minor intergranular porosity was observed, with an average size of 0.8 μm. This porosity, however, was greater than that found in the samples of the S3 system and was evidenced by this system's density, which was 95.4% of the theoretical density, and by its apparent porosity of around 1.5% (Table 1). Figure 2c shows the micrograph of the samples of the S7 system, revealing a heterogeneous microstructure, i.e., grains smaller than 0.5 μm inside a matrix of grains relatively larger than 1 μm, indicating

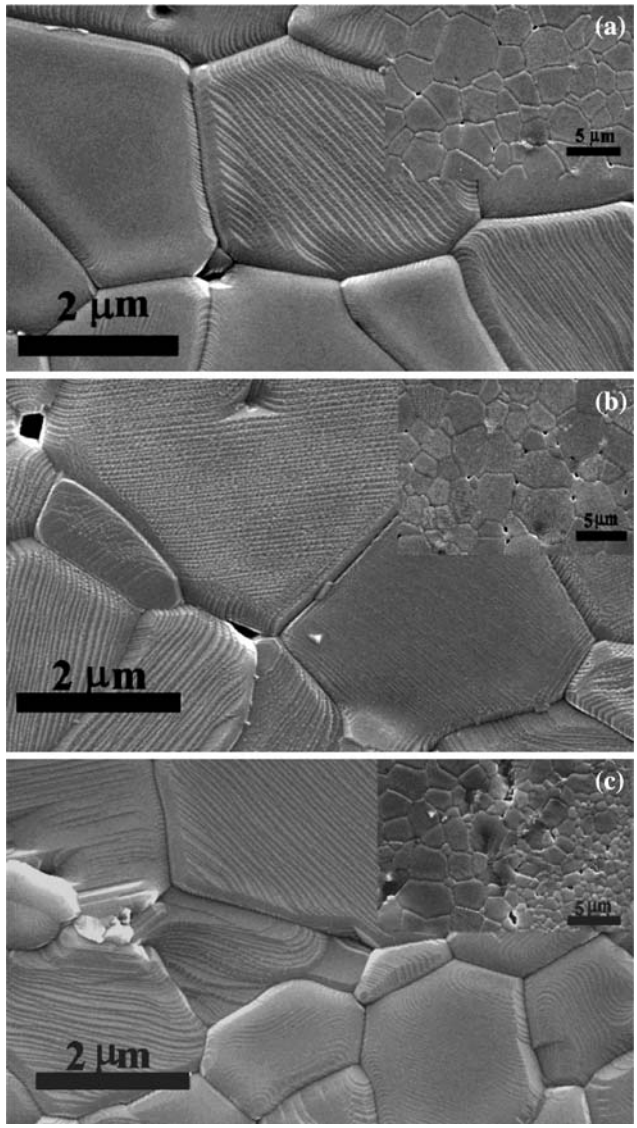

Fig. 2 Scanning electron microscopy micrographs after sintering at 1,200 °C/2 h for the systems: (**a**) S3, (**b**) S5 e (**c**) S7

Table 1 Lattice constant of the powder, average size grain and physic characteristics for the samples of the system $Ni_xZn_{1-x}Fe_2O_4$ sinterized at 1,200 °C/2 h

Systems	S3	S5	S7
Average grain size (μm)	3.36 ± 1.23	2.87 ± 1.11	1.37 ± 0.82
Apparent density (g/cm^3)	5.20 ± 0.01	5.01 ± 0.05	4.88 ± 0.14
Relative density (%)	98.80 ± 0.06	95.40 ± 0.93	92.90 ± 1.00
Apparent porosity (%)	1.00 ± 0.11	1.51 ± 0.48	3.24 ± 1.57
Lattice constant Å, $a = b = c = 8.399$	8.36	8.38	8.40

that the microstructure may be either bimodal or duplex. The average grain size obtained was 1.37 μm, which is equivalent to 48% and 41%, respectively, of the size of certain average grains in the S3 and S5 systems. A larger amount of intergranular porosity was observed in the samples of the S7 system than in the S5 and S3 systems. The grain size and density were found to decrease, while the porosity increased according to the Zn^{2+}concentration. Rana and Abbas [4] demonstrated that both the grain size and porosity decrease with the substitution of Zn in the $Cu_{1-x}Zn_xFe_2O_4$ system prepared by the standard ceramic method.

The average grain size calculated for the S3 (3.36 μm) and S5 (2.87 μm) systems was larger than the values reported by Verma et al. [20] for Ni–Zn ferrite samples with Zn^{2+} concentrations of 0.5 and 0.6 mol% (1.0 and 1.9 μm, respectively) obtained by the citrate precursor method and sintered at 1,200 °C. The S7 system presented a lower average grain size (1.37 μm) than the values reported by Verma et al. [20]. The average grain size value was much lower in the three studied systems than the value obtained for $Ni_{0.4}Zn_{0.6}Fe_2O_4$ (7.8 μm) ferrite samples sintered at 1,200 °C [21] and for $Mn_{0.4}Zn_{0.47}Fe_{0.06}Fe_2O_4$ (10–12 μm) ferrite sintered at 1,350 °C for 5 h [22], both prepared by the conventional oxide mixture method.

Figure 3 shows the dependence of the flux density (B) on the applied magnetic field (H) of the hysteresis loop (B–H) for the sample sintered at 1,200 °C/2 h. Table 2 shows the results of hysteresis parameter measurements (coercivity field, H_c, remanent flux density, B_r, maximum flux density, B_{max}, hysteresis loss, P_H and maximum permeability, μ_{max}) of the S3, S5 and S7 systems sintered at 1,200 °C/2 h. An analysis of the hysteresis loop (B–H) revealed the soft magnetic material characteristics of the S3 and S5 systems. The

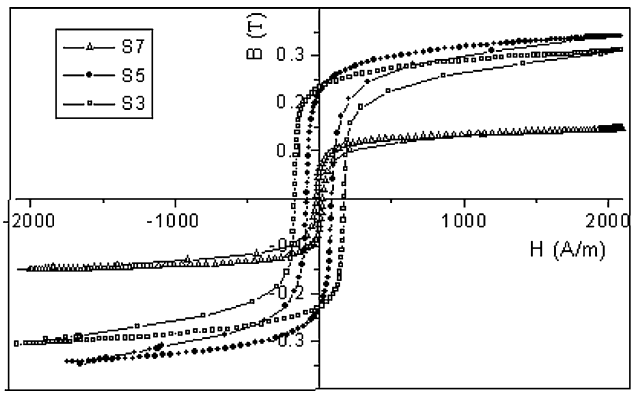

Fig. 3 Room temperature hysteresis loop B–H for samples of the systems S3 ($Ni_{0.7}Zn_{0.3}Fe_2O_4$), S5 ($Ni_{0.5}Zn_{0.5}Fe_2O_4$) and S7 ($Ni_{0.3}Zn_{0.7}Fe_2O_4$) sinterized at 1,200 °C/2 h

hysteresis loop (B–H) of the S3 system was larger (high coercivity field) than that of the S5 system, with magnetic properties relatively lower than those of the S5 system.

Figure 4 shows the dependence of the flux density maximum, B_{max}, and average grain size on the concentration of Zn. The average grain size and, hence, the maximum flux density were found to decrease as the Zn concentration increased. According to Goldman [23], Ni–Zn ferrite should show maximum flux density values ranging from 0.30 to 0.40 T. Thus, Fig. 4, and Tables 1 and 2 show that the maximum flux density value for the S7 system was significantly lower than the values found in the S3 and S5 systems. Because the magnetic properties (coercive field, remanent flux density and loss of hysteresis) are directly related to the maximum flux density, a reduction in those properties is expected. However, this does not mean that the system presented the best results. A similar reduction in the maximum flux density has been reported by other researchers [24–26] in ferrite systems containing high concentrations of Zn, which was the case of the S7 system and was attributed to the phenomenon known as "*spin canting*".

The data in Tables 1 and 2 and Figs. 3 and 4 reveal a decrease in B_{max} with increased Zn substitution. This decrease can be attributed mainly to a decrease in the samples' grain size. It is known that the grain size increases with higher sintering temperatures. It is also known that Zn promotes sintering [26], which results in larger grain sizes. Larger grains tend to consist of a greater number of domain walls. Greater magnetization and permeability are caused by the easiness of the reversible domain wall movement, which requires less energy than domain rotation. Since the number of walls increases with grain size, the contribution of wall movement to magnetization and permeability is greater because domain rotation increases. Therefore, samples with larger grains are expected to possess high magnetization and permeability.

Both magnetization and permeability, therefore, show a direct dependence on grain size. The hysteretic loss is smaller in ferrites with larger grains due to the dependence of magnetization on grain size [27]. However, it should also be pointed out that magnetization and permeability depend on the material's intrinsic characteristics and are, therefore, dependent on the composition and on the cation distribution in the spinel lattice [28].

The average grain size of the S3 system was approximately 14.6% larger than the average grain size of the S5 system. However, as can be observed in Table 1 and Figs. 3 and 4, the samples of the S5 system

Table 2 Hysteresis parameters for the samples of the system $Ni_xZn_{1-x}Fe_2O_4$ sinterized at 1,200 °C/2 h (f = 1 kHz, e = 4.0 mm and H = 2,000 A/m)

H_c (A/m)	168 ± 1.5	93 ± 3.4	17 ± 3.5
B_r (T)	0.25 ± 0.01	0.20 ± 0.05	0.04 ± 0.03
B_{max} (T)	0.33 ± 0.01	0.35 ± 0.01	0.16 ± 0.07
B_r/B_{max}	0.75	0.57	0.25
μ_{max}	494 ± 20	776 ± 88	783 ± 232
P_H (W/kg)	105 ± 59	42 ± 5.4	1.5 ± 0.8

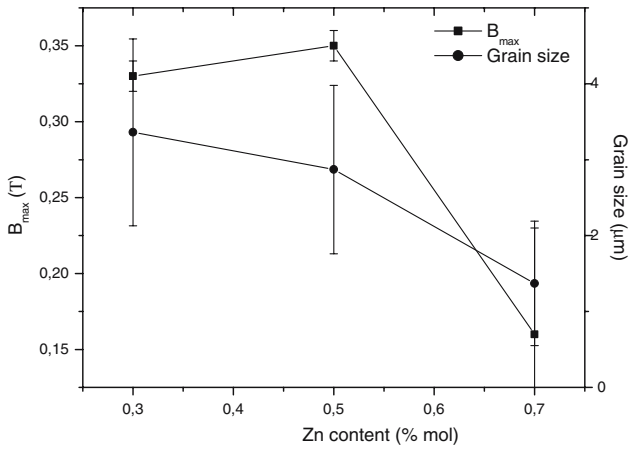

Fig. 4 Variation of the flux density maximum and average grain size with the Zn substitution

displayed a smaller coercive field, less hysteretic loss, and slightly greater magnetization than those of the S3 system. The maximum permeability was about 36% higher than that of the S3 system. These results demonstrate that the intrinsic characteristic (theoretical magnetic moment) of the S5 system prevailed over the microstructural effect of the grain size, resulting in magnetic parameters considerably superior to those of the S3 system, despite the latter's larger grain size.

Both the S3 and S5 systems generally presented excellent magnetic properties, rendering these Ni–Zn ferrite systems suitable for use as soft magnetic devices. The experimental values were found to be congruent with the theoretical ones for Ni–Zn ferrite, which are 0.30–0.40 T for maximum density flux and 10–1,000 for permeability [23]. In the specific case of the S7 system, the ''*spin canting*'' caused a drastic effect that compromised the experimental values of the magnetic parameters.

Conclusions

In conclusion, the results indicate that higher concentrations of Zn^{2+} can influence both the microstructure and the magnetic properties of the material. The increase in the Zn^{2+} concentration caused the constant parameters to rise and led to the formation of single-phase cubic spinel Ni–Zn ferrite and after sintering at 1,200 °C/2 h, the apparent density increased according the Zn^{2+} concentration. The S3 (0.3% of Zn^{2+}) and S5 (0.5% of Zn^{2+}) systems showed a homogeneous microstructure and good magnetic properties. The S7 (0.7% of Zn^{2+}) system showed a bimodal microstructure and drastic effect of ''*spin canting*'', with the values of the magnetic parameter compromised.

Acknowledgements The authors gratefully acknowledge the financial support of CAPES and CNPq (Brazil)

References

1. Ravindernathan P, Patil KC (1987) J Mater Sci 22:3261
2. Igarashi H, Okazaki K (1977) J Am Ceram Soc 60:51
3. Goldman A (1984) Bull Am Ceram Soc 63:582
4. Rana MU, Abbas T (2002) J Magn Magn Mater 246:110
5. El-Sayed AM (2002) Ceram Int 28:363
6. Gonchar A, Gorelik S, Katynkina S, Letyuk L, Ryabov I (2000) J Magn Magn Mater 215–216:221
7. Pramanik P, Pathak A (1994) Bull Mater Sci 17(6):967
8. Costa ACFM, Tortella E, Morelli MR, Kaufman MJ, Kiminami RHGA (2002) J Mater Sci 37:3569
9. Costa ACFM, Tortella E, Morelli MR, Kiminami RHGA (2002) Mater Sci Forum 403:57
10. Costa ACFM (2001) PhD thesis, *In Portuguese*, Universidade Federal de São Carlos, Brazil
11. Sekar MMA, Patil KC (1992) J Mater Chem 2(7):739
12. Kiminami RHGA (2001) J KONA 19:156
13. Sousa VC de, Castro MS, Morelli MR, Kiminami RHGA (2002) J Mater Sci Mater Electron 13:319
14. Segadães AM, Morelli MR, Kiminami RHGA (1998) J Eur Ceram Soc 18(7):771
15. Ravindranathan CS, Hong P, Agraval DK, Roy R (1994) J Mater Sci Lett 12:1072
16. Ravindranathan P, Komarneni S, Roy R, (1993) J Mater Sci Lett 12:369
17. Dhas A, Patil KC (1994) Ceram Int 20:57
18. Jain SR, Adiga KC, Pai Verneker VR (1981) Combust Flame 40:71
19. Prakash C, Baijal JS (1984) Solid State Commun 50:557
20. Verma A, Goel TC, Mendiratta RG, Kishan P (2000) J Magn Magn Mater 208:13
21. Pyun SI, Baek JT (1985) Am Ceram Soc Bull 64(4):602
22. Ahns SJ, Yoon CS, Yoon SG, Kim CK, Byun TY, Hong KS (2001) Mater Sci Eng B84:146
23. Goldman A (1991) Magnetic Ceramics (Ferrites), Ferrite Technology Worldwide Inc. Engineered Materials Handbook, Ceramics and Glasses, ASM International 4, p 1161
24. Gorte EW (1954) Philips Res Rep 9:295
25. Bercoff PG, Bertorello HR (2000) J Magn Magn Mater 213:56
26. Znidarsic A, Drofenik M (1996) IEEE Trans Magn 32(3):1941
27. Zhiyuan L, Maoren X, Qingqiu Z (2000) J Magn Magn Mater 219:9
28. Bhise BV, Dongare MB, Patil SA, Sawant SR (1991) J Mater Sci Lett 10:922